Scaling an Axial Flux Permanent Magnet Motor for Different Electrified Aviation Applications

Sri Vignesh Sankarraman
Electrical and Computer Engineering
The University of Texas at Dallas
Richardson, TX, USA
srivignesh.sankarraman@utdallas.edu

Sina Khalesidoost
Electrical and Computer Engineering
The University of Texas at Dallas
Richardson, TX, USA
sina.khalesidoost@utdallas.edu

Dorsa Talebi
Electrical and Computer Engineering
Texas A&M University
College Station, TX, USA
dorsa.talebi@tamu.edu

S. Mehdi Seyedi
Electrical and Computer Engineering
Texas A&M University
College Station, TX, USA
mehdiseyedi@tamu.edu

Matthew Gardner
Electrical and Computer Engineering
The University of Texas at Dallas
Richardson, TX, USA
matthew.gardner@utdallas.edu

Abstract: This paper presents a base topology of an axial flux permanent magnet (AFPM) motor selected for a fully electric powertrain for a single-aisle aircraft based on the specifications provided in the Aviation-Class Synergistically Cooled Electric-motors with iNtegrated Drives (ASCEND) project from the Advanced Research Projects Agency-Energy (ARPA-E). The ASCEND motor is assessed for scalability to fit other aircraft profiles. The scaled design's performance is compared with the ASCEND design to understand the effect of scaling and avenues of improvement. The SCEPTOR project requires 54% as much speed and 83% as much torque as ASCEND; at these specifications, the SCEPTOR motor is 1.6% less efficient than the ASCEND motor. This is because the DC copper losses are a larger fraction of the output power. While the core and magnet losses are lower than the ASCEND design at a greatly reduced speed, these were already smaller than the copper losses. The SUSAN design requires a 36% increase in speed and a 317% increase in torque. The SUSAN motor is 0.7% less efficient than the ASCEND motor due to the dominant AC losses. At this larger scale, the active torque and power density were increased significantly, whereas by scaling down the active torque and power density were reduced. ***Index Terms*—Axial flux permanent magnet machine, YASA, electric power train, scaling**

I. Introduction

The drive towards electrification of aircraft to achieve zero emissions is radically changing the aviation industry. The aviation industry is moving from more electric aircraft (MEA) to all-electric aircraft [1], [2]. Since all-electric aircraft are still in their inception stages, much research is conducted on making aircraft with different flight profiles, from inter-city travel to trans-continental travel. The range of these flights depends significantly on battery energy storage. However, electric motors are also a key component in electric aircraft design [3], [4]. The weight and volume of electric motors are vital parameters for aerospace applications; optimizing these parameters is paramount. Motor efficiency also affects how much battery energy storage is required. The combined high power and reduced volume requirements make power density one of the most critical parameters for motors designed for aerospace applications. Motor technology requires significant improvements in power density over the current state of the art [5].

Axial flux permanent magnet (AFPM) motors can achieve high power densities [6], [7]. In particular, the yokeless and segmented armature (YASA) topology allows the removal of the stator yoke and the use of high current densities [8]. The short end turns help lower the winding lengths, thereby saving mass and increasing efficiency. In this topology, the core loss can be further reduced by replacing the yoke with an additional rotor [9]. Cobalt steel's higher saturation flux density can reduce the required stator current compared to silicon steel, which increases power density and efficiency [10], [11].

ARPA-E focuses on building a fully electric powertrain for a single-aisle aircraft with a motor that provides a peak power of 250 kW at 5000 RPM during take-off through their ASCEND project [12]. Previously, a YASA design has been specified for this power [13]. This paper will present similar YASA designs for other electric aircraft applications to evaluate the scalability of the topology. This topology will be scaled to aircraft with lower and higher power requirements.

This paper aims to study the scalability of the proposed YASA design, which will be given in section 2. Section 3 scales the design to an aircraft SCEPTOR from NASA with a motor requirement with lower power. Similarly, section 4 scales the design to another NASA aircraft design, SUSAN, with a higher motor power requirement. Section 5 discusses the results from sections 3 and 4 and compares the efficiency and power density of the motors with the base ASCEND design given in Section 2.

This work was supported by the Department of Energy under Award DE-AR0001356 [DOI: 10.1109/IEMDC47953.2021.9449611].

TABLE I
ASCEND PROGRAM POWERTRAIN TARGETS

Takeoff mechanical shaft power output	$\geq$ 250 kW
Maximum rotational speed at takeoff	5,000 RPM
Specific power at takeoff	$\geq$ 12 kW/kg
Takeoff and climb average efficiency	$\geq$ 93%
Cruise mechanical shaft power output	$\geq$ 83 kW
Cruise rotational speed	3,500 RPM - 4,500 RPM
Average cruise efficiency	$\geq$ 93%

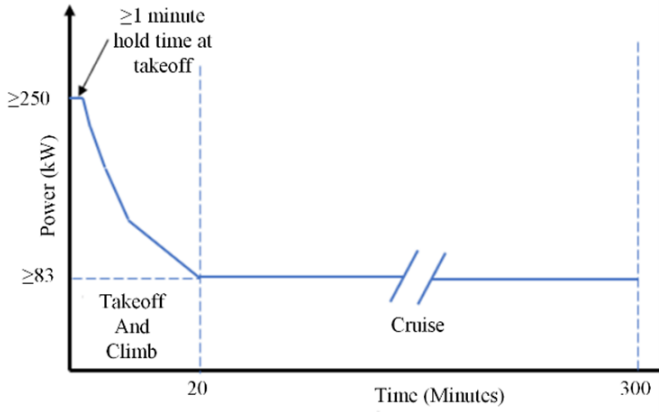

Fig. 1. ASCEND program flight profile

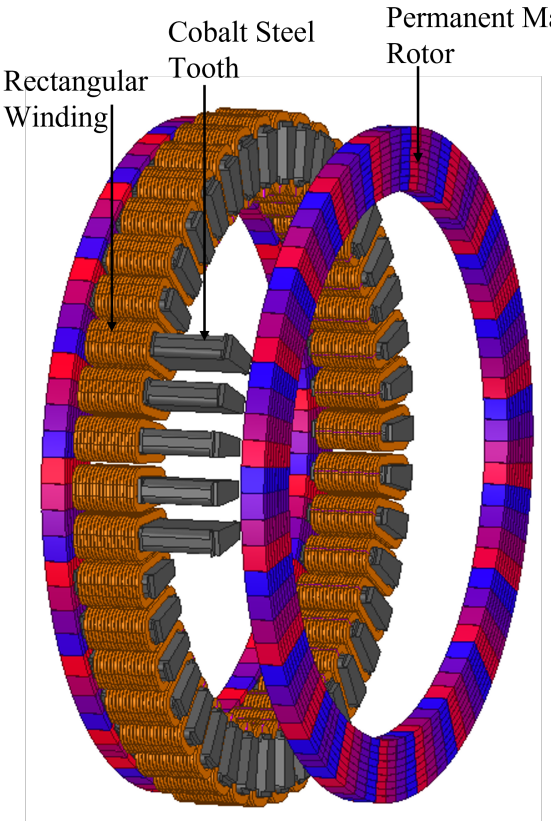

Fig. 2. ASCEND design with 40 poles and 42 teeth

II. MOTOR DESIGN BASED ON THE ASCEND SPECIFICATIONS

ARPA-E defined the target specifications shown in Table I [12] through the ASCEND program to achieve a powertrain (motor, inverter, and thermal management) system that greatly advances the state-of-the-art [5]. Per the flight profile shown in Fig. 1, the peak power of 250 kW at 12 kW/kg and 5000 RPM must be sustained for a minute, after which the power gradually ramps down over 20 minutes to reach the cruise power of 83 kW.

The AFPM motor proposed for this design is shown in Fig. 2. Using a fractional slot concentrated winding (FSCW) provides advantages like improved fill factor and fault tolerance [8], [14]. The YASA topology removes the stator yoke and replaces it with an additional rotor, which reduces the core losses [15]. Due to its higher permeability and lower losses, cobalt steel is the preferred material for the stator teeth. To further minimize eddy current losses in the rotor, the permanent magnets (PMs) are segmented. The number of segments was optimized, and the optimized PMs have nine segments each [13]. Furthermore, using a Halbach array, the rotor flux has a return path within the PMs, eliminating the need for a heavy rotor back iron. Instead, PMs are mounted on a lightweight carbon fiber-reinforced polymer [16]. The Halbach array also makes the flux distribution more sinusoidal. The copper fill factor is increased using wires with rectangular cross-sections. The rectangular wires also provide a flat end-winding surface. On the outer end-winding surface are heatsinks with mini-channels through which a coolant flows, and on the inner end-winding, phase change thermal energy storage is used to dissipate the excess heat generated during takeoff [17].

A parametric sweep using commercial finite element analysis (FEA) software (ANSYS Maxwell) was employed to determine the optimal design for the ASCEND project. The initial parametric sweep is given in Table. II.

TABLE II
PARAMETRIC SWEEP RANGE FOR INITIAL DESIGN

Name	Description	Values	Units
Slots/PP	Slots pole pair combinations	12/5,18/8,24/10,24/11,24/14,27/12	
		30/14,36/16,36/17,42/20,45/24,48/26	
R_{2s}	Stator Teeth Outer Radius	120,135	mm
R_{1s}	Stator Teeth Inner Radius		
	For R2s = 120	80,85,90,95	mm
	For R1s = 135	100,105,110,115	mm
L_s	Stator Teeth Axial Length		
	For R2s = 120	35,40,45,50	mm
	For R1s = 135	25,30,35,40	mm
FF_{cu}	Copper Fill Factor	0.8	
k_{tw}	Tooth Width to Tooth Pitch Ratio	0.4,0.5,0.6	
J	RMS Current Density	29.7,35.6	A/mm^2
A_g	Airgap thickness	1	mm
L_r	Magnet Axial Thickness	5,10,15,20	mm

TABLE III
FINAL DESIGN FOR ASCEND SPECIFICATION

Name	Description	Value	Units
	Slot/Pole	42/20	
Ls	Stator Length	30	mm
R1s	Stator Inner Radius	115	mm
R2s	Stator Outer Radius	135	mm
Ag	Airgap	1	mm
Lr	Magnet Axial Length	10	mm
ktw	Tooth Width to Tooth Pitch Ratio	0.6	
J	RMS Current Density	35.6	A/mm2
wt	Take-Off Speed	5000	RPM
wc	Cruise Speed	4000	RPM

Various combinations from this design space were simulated using Ansys Maxwell magnetostatic simulations. The results from the static simulation were used to narrow down the designs, which were then analyzed using transient simulations to identify the torque, loss, and efficiency. The optimal parameters from the transient simulations are shown in Table III [13]. On the material side, the stator tooth is simulated with two different materials, grain oriented silicon steel and cobalt steel. Cobalt steel's higher saturation flux density helps achieve the required torque with a lower current value, thereby reducing winding losses. Due to the ease of manufacturing, edge-bent windings with rectangular cross-sections are used. The windings are simulated at 250°C, accounting for the heat flux through the end windings, which was calculated to be 2.8 W/mm^2 at takeoff. Neodymium Iron Boron (NdFeB) N48SH grade magnets are chosen for the rotor to withstand predicted magnet temperatures up to 100°C.

This motor is kept as the base design, and the motor parameters are scaled to fit two different aircraft specifications, SCEPTOR and SUSAN.

III. SCALED DESIGN BASED ON THE SCEPTOR SPECIFICATIONS

The NASA SCEPTOR program has built a fully electric powertrain for a test aircraft [18]. Per the SCEPTOR design, the aircraft has 12 small high-lift motors and two larger cruise motors. The high-lift motors are used only during take-off and are inactive while cruising. To evaluate the scalability of the topology used for the ASCEND project, a similar design will be selected to meet the specifications of the cruise motor for the SCEPTOR program.

Table IV provides the target specifications of the cruise motor used for the SCEPTOR aircraft [18]. Compared to the ASCEND motor, the maximum torque is reduced by about 17%, and the maximum speed is reduced by 46%. Thus, the peak power requirement is reduced by 55%.

The previous design space used for the ASCEND motor was filtered to find points that satisfied the new scaled parameters.

TABLE IV
SCEPTOR DESIGN REQUIREMENTS

Metric	Target
Motor Mass	22 kg
Speed	2700 RPM max
Torque	400 Nm max
Battery Voltage	400-525 V

Based on initial magnetostatic simulations, ten designs were selected to produce at least 400 Nm torque, have an active mass of less than 7.5 kg, and have no more than 20 pole pairs (to avoid excessive manufacturing complexity). For each design, the number of turns per coil in the stator winding is selected to achieve a voltage suitable for the range of DC bus voltages in Table 2 without having an axial length for each turn of less than 1 mm (to avoid impractical windings). This yielded 12 possible cases. (There were multiple acceptable turn counts for a few of the original ten designs.) Using 3D transient models in Ansys Maxwell, the 12 cases were simulated to determine the winding loss, core loss, and magnet loss. The SCEPTOR models were simulated with the same materials used in the ASCEND motor model. The heat flux generated from the windings for all the SCEPTOR aircraft cases is lower than the ASCEND model. Therefore, as a conservative estimate, the windings are still assumed to have a temperature of 250°C

The various loss results obtained from the simulations are shown in Figs. 3-5. The number of turns and the DC bus voltage for the different design cases can be seen in Figs. 6 & 7. Since the winding loss is the most dominant type of loss, the case with the least winding loss and the highest efficiency is chosen from Fig. 3 for comparison. The winding loss contains the AC and the DC losses in the windings. The corresponding core and magnet losses can be seen in Fig. 4 & 5.

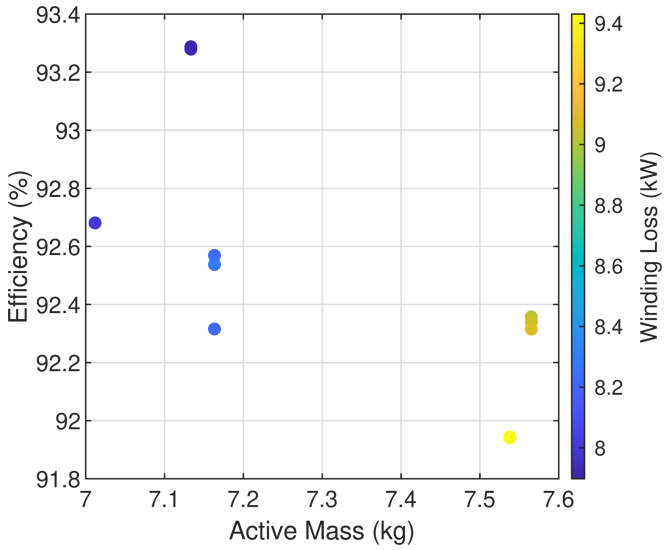

Fig. 3. Winding loss for different SCEPTOR design cases

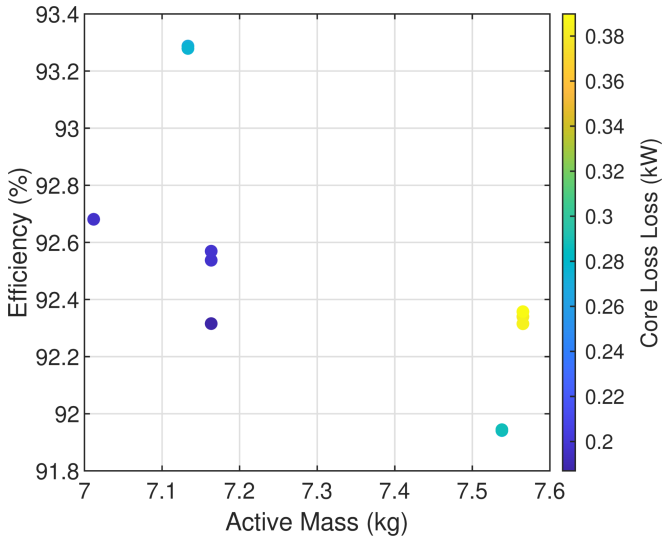

Fig. 4. Core loss for different SCEPTOR design cases

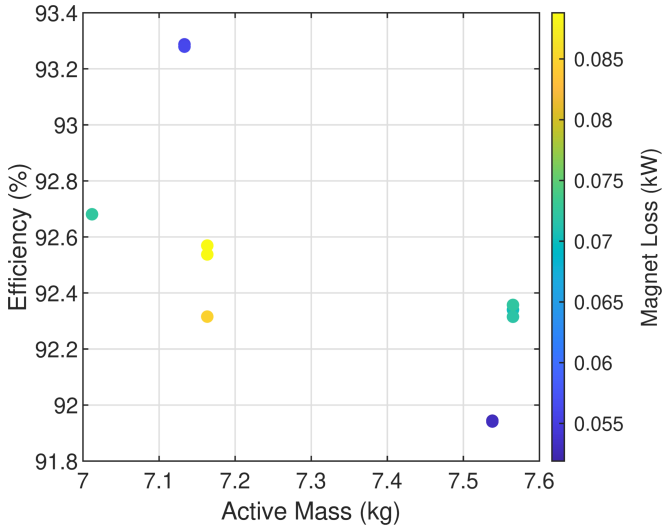

Fig. 5. Magnet loss for different SCEPTOR design cases

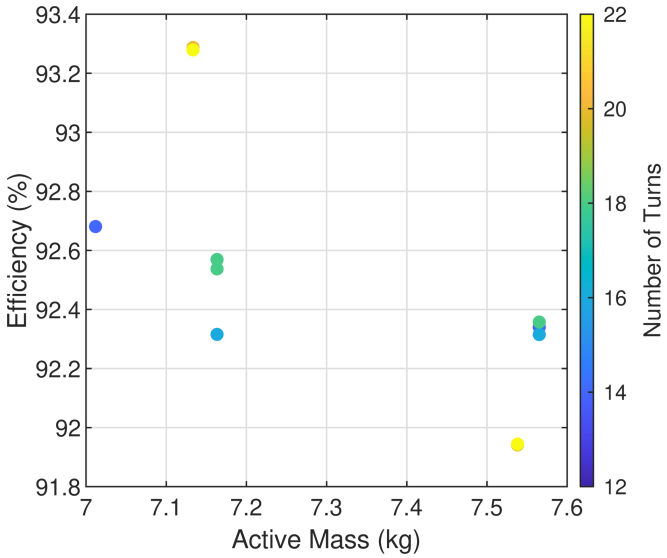

Fig. 6. Number of turns for different SCEPTOR design cases

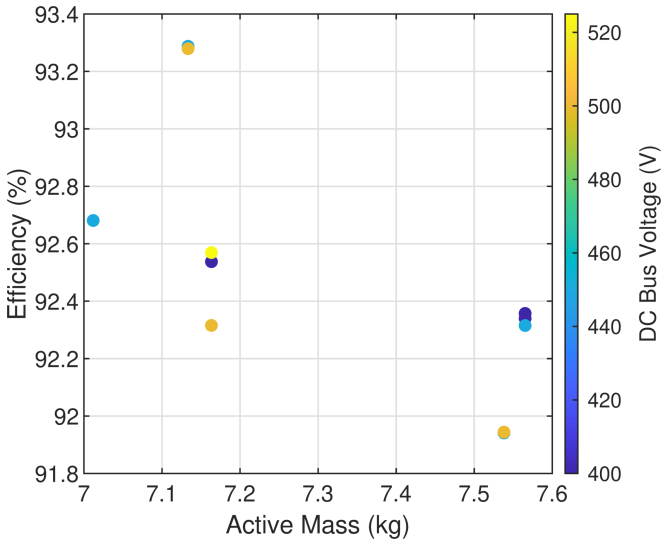

Fig. 7. DC bus voltage for different SCEPTOR design cases

From Figs. 3-7. It can be seen that two design cases have approximately 93.3% efficiency. The difference between these two cases is the number of turns and the DC bus voltage. Since a higher DC bus voltage is preferable from a system-level perspective to reduce losses in the aircraft cables, the design case with the higher (500V) DC bus voltage is chosen.

IV. Scaled Design based on the SUSAN Specifications

The SCEPTOR specification was based on scaling the ASCEND design down. To scale up the ASCEND parameters, a second specification was chosen. The NASA Glenn research center proposes a megawatt-class motor for their Electrified Aircraft Propulsion (EAP) intended for a single-aisle aircraft. The target specifications are provided in Table V [19].

The parametric sweep used for the ASCEND design is extended to have larger geometric parameters to increase the torque produced. The maximum speed is increased by 36% and the maximum torque is increased by 317%; thereby, the maximum power is increased by 460% more than the ASCEND target specifications.

TABLE V
SUSAN Design Requirements

Requirement	Target
Output Power	1.4 MW
Electromagnetic Power Density	16 kW/kg
Rated Speed	6800 RPM
Rated Torque	1.97 kNm

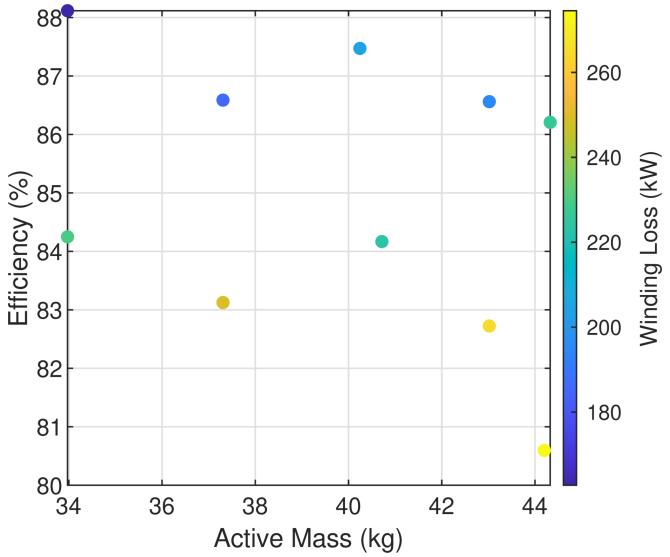

Fig. 8. Winding loss for different SUSAN design cases

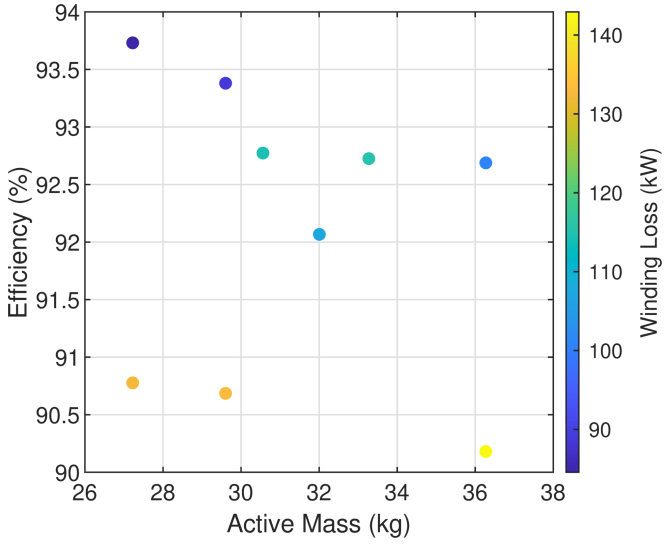

Fig. 9. Winding loss for different SUSAN design cases with tooth tips and aluminum conductors

From the parametric sweep similar to the SCEPTOR model, seven design cases were filtered from the magnetostatic simulation to satisfy this target specification. Each design case produces at least 1.97 kNm of torque and the electromagnetic active mass was filtered to be less than 45 kg, keeping the pole pairs constant. The number of turns is calculated by ensuring the chosen DC bus voltages are feasible. The current density is also scaled to produce the required 1.97 kNm torque. DC bus voltages between 1200V to 2000V are used to calculate a suitable number of turns. The design cases with very high winding axial lengths or large (¿4) ratios between winding tangential widths and axial thicknesses are considered impractical. After filtering the impractical cases, these 7 cases yield 10 cases with different numbers of turns. The transient models of these 10 cases were simulated using 3D FEA to calculate the different losses.

Fig. 8 shows the different design cases' winding (AC + DC) losses. From these losses, it can be speculated that most of the losses would be AC due to the large size of each turn. To reduce the effect of AC winding losses, rectangular soft magnetic composite (SMC) tooth tips are used to shield the windings from the flux from the rotor, which reduces the eddy currents in the windings. Due to their lower electrical conductivity, aluminum (1350 alloy) conductors are also used to reduce AC losses. The use of aluminum windings also helps in reducing the actve weight of the motor. The design cases are rerun after including the tooth tips and the aluminum windings. The windings are simulated at the same temperature as ASCEND and SCEPTOR due to lower heat flux from the end windings than the ASCEND design.

Figs. 9-11 provides the different losses generated in each design case. Figs. 12 and 13 show the number of turns and the DC bus voltage for each design case. The most efficient design (93.7%) that generates the required torque is chosen

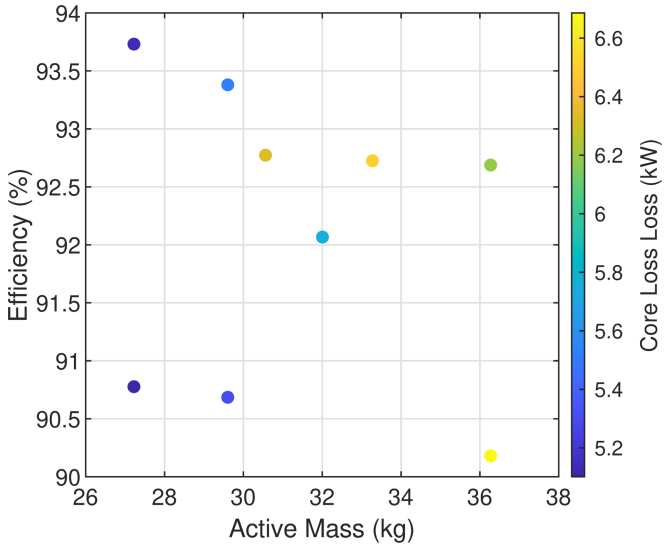

Fig. 10. Core loss for different SUSAN design cases with tooth tips and aluminum conductors

from Fig for comparison. 9.

V. Comparison of the Best Designs for the Three Specifications

In the previous three sections, the design of the dual rotor axial flux motor for three different aircraft specifications was discussed. The design that yielded the best efficiency in all three models was chosen. Table VI compares the best designs for ASCEND, SCEPTOR, and SUSAN in terms of the losses, DC bus voltage, torque, and power Density.

Table VI shows that for the SUSAN design, the major contributor to the winding loss is the AC losses. For the ASCEND and SCEPTOR designs, the DC losses are more dominant. By scaling up the power level, better torque densities and

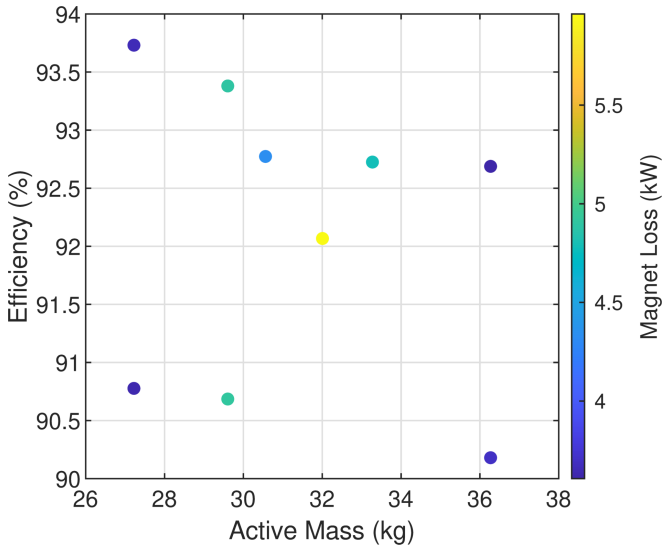

Fig. 11. Magnet loss for different SUSAN design cases with tooth tips and aluminum conductors

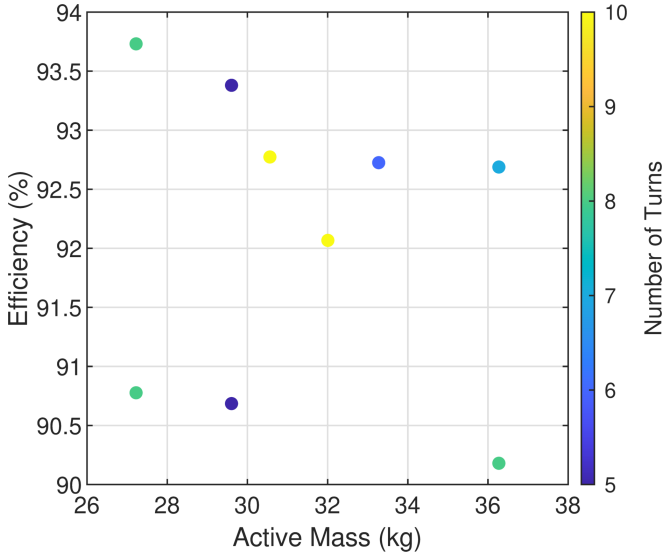

Fig. 12. Number of turns for different SUSAN design cases with tooth tips and aluminum conductors

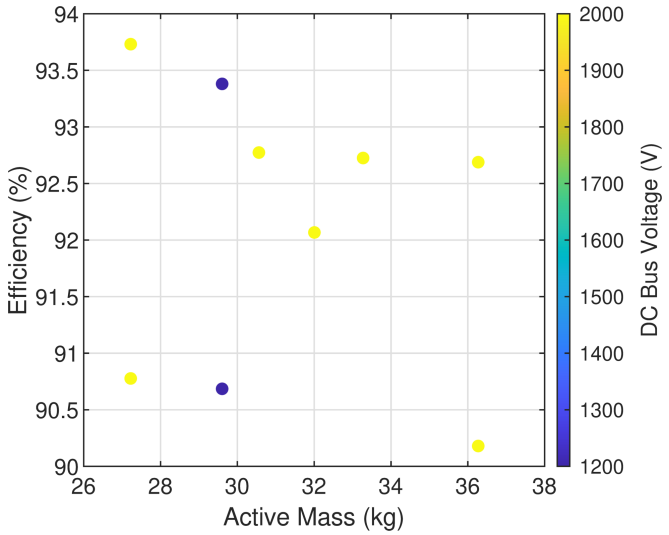

Fig. 13. DC bus voltage for different SUSAN design cases with tooth tips and aluminum conductors

TABLE VI
COMPARISON OF THE BEST DESIGNS FOR THE THREE SPECIFICATIONS

Parameters	ASCEND	SCEPTOR	SUSAN
AC Winding Loss (P.U)	0.0072	0.0085	0.0484
DC Winding Loss (P.U)	0.04	0.062	0.012
Core Loss (P.U)	0.0077	0.0024	0.0037
Magnet Loss (P.U)	0.0012	0.0005	0.0026
DC Bus Voltage (V)	1000	500	2000
Torque (Nm)	477	400	1970
Power (kW)	250	113	1400
Efficiency (%)	94.9	93.3	94.2
Active Torque Density (Nm/kg)	63.26	56	72.43
Active Power Density (kW/kg)	33.16	15.83	51.47
Inner Diameter (mm)	220	220	440
Outer Diameter (mm)	270	270	520
Slots/Pole	42/40	42/40	42/40
Stator Length (mm)	34.66	25	30
Magnet Axial Thickness (mm)	10	10	30
Air gap thickness (mm)	1	1	2
Current Density (Arms/mm2)	35.69	35.69	18.65

power densities can be achieved. At this current design level, the SUSAN design is able to achieve efficiencies very close to the ASCEND design. The efficiency can be improved by reducing the AC losses, which can be achieved by optimizing the geometry and the tooth tips [20].

VI. Conclusion

An axial flux dual-rotor axial flux motor was designed and scaled for three different power levels, 113 kW (SCEPTOR), 250 kW (ASCEND), and 1.4 MW (SUSAN). The comparison yields some conclusions:

- Scaling to a lower power reduces the efficiency, active torque, and power density. In this case, the power density varies more than the torque density, due to the different speeds at different power levels.
- For the large scale design (SUSAN), the large winding cross-sections result in large AC losses in the winding.
- The AC losses were reduced by including tooth tips and aluminum windings for the SUSAN design, which can be optimized further to improve efficiency.
- At higher power levels due to thicker magnets, the magnet losses increase, warranting the need for increasing segmentation of the magnets.
- The core loss is the higher in the ASCEND design relative to the other designs; the AC winding losses dominate in the SUSAN design, which has the highest speed; and the DC losses dominate in the SCEPTOR design, which has the lowest speed.

ACKNOWLEDGMENT

The authors would like to thank ANSYS for their support of the EMPE lab through the provision of FEA software. Portions of this research were conducted with the advanced computing resources provided by Texas A&M High Performance Research Computing. This report was prepared as an account of work sponsored by an agency of the United States Government. Neither the United States Government nor any agency thereof, nor any of their employees, makes any warranty, express or implied, or assumes any legal liability or responsibility for the accuracy, completeness, or usefulness of any information, apparatus, product, or process disclosed, or represents that its use would not infringe privately owned rights. Reference herein to any specific commercial product, process, or service by trade name, trademark, manufacturer, or otherwise does not neces- sarily constitute or imply its endorsement, recommendation, or favoring by the United States Government or any agency thereof. The views and opinions of authors expressed herein do not necessarily state or reflect those of the United States Government or any agency thereof.

REFERENCES

[1] N. Thapa, S. Ram, S. Kumar, and J. Mehta, "All electric aircraft: A reality on its way," *Materials Today: Proceedings*, vol. 43, pp. 175–182, 2021.

[2] C. E. Jones, P. Norman, G. M. Burt, C. Hill, G. Allegri, J. Yon, I. Hamerton, and R. Trask, "A Route to Sustainable Aviation: A Roadmap for the Realization of Aircraft Components With Electrical and Structural Multifunctionality," *IEEE Trans. Transport. Electrific.*, vol. 7, no. 4, pp. 3032–3049, Dec 2021.

[3] A. Barzkar and M. Ghassemi, "Components of electrical power systems in more and all-electric aircraft: A review," *IEEE Trans. Transport. Electrific.*, vol. 8, no. 4, pp. 4037–4053, 2022.

[4] P. Alvarez, M. Satrustegui, I. Elosegui, and M. Martinez-Iturralde, "Review of High Power and High Voltage Electric Motors for Single-Aisle Regional Aircraft," *IEEE Access*, vol. 10, pp. 112 989–113 004, 2022.

[5] F. Martini, "Siemens develops world-record electric motor for aircraft," 2015, publication Title: Siemens. [Online]. Available: https://press.siemens.com/global/en/pressrelease/siemens-develops-world-record-electric-motor-aircraft

[6] P. Ojaghlu and A. Vahedi, "A New Axial Flux Permanent Magnet Machine," *IEEE Trans. Magn.*, vol. 54, no. 1, pp. 1–6, 2018.

[7] J. Z. Bird, "A Review of Electric Aircraft Drivetrain Motor Technology," *IEEE Trans. Magn*, vol. 58, no. 2, pp. 1–8, 2022.

[8] N. Taran, G. Heins, V. Rallabandi, D. Patterson, and D. M. Ionel, "Evaluating the Effects of Electric and Magnetic Loading on the Performance of Single- And Double-Rotor Axial-Flux PM Machines," *IEEE Trans. Ind. Appl.*, vol. 56, no. 4, pp. 3488–3497, 2020.

[9] N. Taran, G. Heins, V. Rallabandi, D. Patterson, and D. Ionel, "Torque Production Capability of Axial Flux Machines with Single and Double Rotor Configurations," in *Proc. IEEE Energy Conver. Congr. Expo*, 2023.

[10] A. Krings, A. Boglietti, A. Cavagnino, and S. Sprague, "Soft Magnetic Material Status and Trends in Electric Machines," *IEEE Trans. Ind. Electron.*, vol. 64, no. 3, pp. 2405–2414, 2017.

[11] M. Centner and U. Schafer, "Optimized Design of High-Speed Induction Motors in Respect of the Electrical Steel Grade," *IEEE Trans. Ind. Electron.*, vol. 57, no. 1, pp. 288–295, Jan 2010.

[12] "DE-FOA-0002238: Aviation-class synergistically cooled electric-motors with integrated drives (ASCEND)," 2019, publication Title: Dept. Energy, Adv. Res. Projects Agency Energy.

[13] D. Talebi, M. C. Gardner, S. V. Sankarraman, A. Daniar, and H. A. Toliyat, "Electromagnetic design characterization of a dual rotor axial flux motor for electric aircraft," *IEEE Trans. Ind. Appl.*, vol. 58, no. 6, pp. 7088–7098, 2022.

[14] B. Zhang, Y. Wang, M. Doppelbauer, and M. Gregor, "Mechanical construction and analysis of an axial flux segmented armature torus machine," in *Proc. Int. Conf. Elect. Mach.*, 2014, pp. 1293–1299.

[15] N. Taran, G. Heins, V. Rallabandi, D. Patterson, and D. M. Ionel, "Systematic Comparison of Two Axial Flux PM Machine Topologies: Yokeless and Segmented Armature versus Single Sided," in *Proc. IEEE Energy Conver. Congr. Expo*, 2019, pp. 4477–4482.

[16] C. Wiley, D. Talebi, S. V. Sankarraman, M. C. Gardner, and M. Benedict, "Design of a carbon fiber rotor in a dual rotor axial flux motor for electric aircraft," in *Proc. IEEE Energy Conver. Congr. Expo*, 2022, pp. 1–8.

[17] N. Malone, S. Chakravarty, S. Zhang, D. Talebi, S. V. Sankarraman, E. Pool, D. Park, E. T. Iverson, C. Wiley, P. Shamberger, D. Antao, M. C. Gardner, H. Toliyat, P. Enjeti, B. Rasmussen, J. Grunlan, B. Moble, and J. Felts, "Investigation of Mass Savings Potential of Zeolite Integrated Motor Thermal Management Systems in All-Electric Commercial Aircraft," *Proc. ASME International Mechanical Engineering Congress and Exposition*, vol. 8, pp. 1–16, 2022.

[18] A. Dubois, M. van der Geest, J. B. Bevirt, S. Clarke, R. J. Christie, and N. K. Borer, "Design of an electric propulsion system for SCEPTOR," *Proc. AIAA Aviation Technology, Integration, and Operations Conference*, pp. 1–29, 2016.

[19] R. Jansen, Y. De Jesus-Arce, P. Kascak, R. W. Dyson, A. Woodworth, J. J. Scheidler, R. Edwards, E. J. Stalcup, J. Wilhite, K. P. Duffy, P. Passe, and S. McCormick, "High Efficiency Megawatt Motor Conceptual Design," in *Proc. AIAA Joint Propulsion Conference*, Jul. 2018.

[20] D. Talebi, S. V. Sankarraman, M. Seyedi, S. Khalsidoost, N. Martin, M. Gardner, and H. Toliyat, "Efficient design and material strategies for high power density axial flux permanent magnet motors," in *Proc. IEEE Energy Conver. Congr. Expo*, 2023.